Published in final edited form as:
*Nat Med*. 2014 November ; 20(11): 1340–1347. doi:10.1038/nm.3646.

# A next-generation dual-recombinase system for time and host specific targeting of pancreatic cancer

**Nina Schönhuber**[#1], **Barbara Seidler**[#1], **Kathleen Schuck**[#1], **Christian Veltkamp**[#1], **Christina Schachtler**[1], **Magdalena Zukowska**[1], **Stefan Eser**[1], **Thorsten B. Feyerabend**[2], **Mariel C. Paul**[1], **Philipp Eser**[3], **Sabine Klein**[1], **Andrew M. Lowy**[4], **Ruby Banerjee**[5], **Fangtang Yang**[5], **Chang-Lung Lee**[6], **Everett J. Moding**[7], **David G. Kirsch**[6,7], **Angelika Scheideler**[8], **Dario R. Alessi**[9], **Ignacio Varela**[10], **Allan Bradley**[5], **Alexander Kind**[11], **Angelika E. Schnieke**[11], **Hans-Reimer Rodewald**[2], **Roland Rad**[1,5,12], **Roland M. Schmid**[1,12], **Günter Schneider**[1], and **Dieter Saur**[1,12]

[1]Department of Internal Medicine II, Klinikum rechts der Isar, Technische Universität München, München, Germany.

[2]German Cancer Research Center (DKFZ), Division for Cellular Immunology, Heidelberg, Germany.

[3]Gene Center and Department of Biochemistry, Center for Integrated Protein Science CIPSM, Ludwig-Maximilians-Universität München, München, Germany

[4]Moores Cancer Center, Division of Surgical Oncology, University of California San Diego, La Jolla, California, USA.

[5]Wellcome Trust Sanger Institute, Genome Campus, Hinxton, Cambridge, UK.

[6]Department of Radiation Oncology, Duke University Medical Center, Durham, North Carolina, USA.

[7]Department of Pharmacology and Cancer Biology, Duke University Medical Center, Durham, North Carolina, USA.

[8]Helmholtz Zentrum München, Research Unit Comparative Medicine, Neuherberg, Germany.

[9]MRC Protein Phosphorylation Unit, University of Dundee, Dundee, UK.

[10]Instituto de Biomedicina y Biotecnología de Cantabria (CSIC-UC-Sodercan), Departamento de Biología Molecular, Universidad de Cantabria, Santander, Spain.

[11]Livestock Biotechnology, Technische Universität München, Freising, Germany.

Correspondence should be addressed to D.S. (dieter.saur@lrz.tum.de)..

AUTHOR CONTRIBUTIONS

B.S. and D.S. designed research; N.S., B.S., K.S., C.V., C.S., M.Z., S.E., M.C.P., P.E., S.K., R.B., F.Y., A.S., I.V., R.R., G.S., and D.S., performed research; T.B.F., A.M.L., C.L.L, E.J.M, D.G.K., A.S., D.R.A., I.V., A.B., A.K., A.E.S., H.R.R., R.R. and R.M.S. contributed new reagents/analytic tools; N.S., B.S., K.S., C.V., C.S., M.Z., S.E., M.C.P., P.E., S.K., R.B., F.T.Y., I.V., R.R., G.S. and D.S. analyzed data; and B.S. and D.S. wrote the paper. N.S., B.S., K.S., and C.V. contributed equally to this manuscript.

COMPETING FINANCIAL INTERESTS

The authors declare no competing financial interests.

**Accession codes.** Microarray data are available in the EMBL-EBI ArrayExpress database under accession number E-MTAB-2551.

[12]German Cancer Research Center (DKFZ) and German Cancer Consortium (DKTK), Heidelberg, Germany.

[#] These authors contributed equally to this work.

## Abstract

Genetically engineered mouse models (GEMMs) have dramatically improved our understanding of tumor evolution and therapeutic resistance. However, sequential genetic manipulation of gene expression and targeting of the host is almost impossible using conventional Cre-*loxP*–based models. We have developed an inducible dual-recombinase system by combining flippase-*FRT* (Flp-*FRT*) and Cre-*loxP* recombination technologies to improve GEMMs of pancreatic cancer. This enables investigation of multistep carcinogenesis, genetic manipulation of tumor subpopulations (such as cancer stem cells), selective targeting of the tumor microenvironment and genetic validation of therapeutic targets in autochthonous tumors on a genome-wide scale. As a proof of concept, we performed tumor cell–autonomous and nonautonomous targeting, recapitulated hallmarks of human multistep carcinogenesis, validated genetic therapy by 3-phosphoinositide-dependent protein kinase inactivation as well as cancer cell depletion and show that mast cells in the tumor microenvironment, which had been thought to be key oncogenic players, are dispensable for tumor formation.

Pancreatic ductal adenocarcinoma (PDAC) is a fearsome disease, with a mortality rate >95% that has remained unchanged for decades[1].

GEMMs that faithfully recapitulate the histological, molecular, genetic and clinical hallmarks of human PDAC have been developed[2–5]. All are based on pancreatic expression of oncogenic $Kras^{G12D}$ or $Kras^{G12V}$, which induce pancreatic intraepithelial neoplasias (PanINs) that progress to aggressive metastatic PDAC[2–4,6–9]. These GEMMs have elucidated the natural biology of pancreatic cancer, revealed potential diagnostic and therapeutic targets[10,11] and highlighted the importance of the tumor stroma for PDAC maintenance, immune evasion and drug resistance[5,12–14].

However, classical Cre-*loxP*–based GEMMs rely on a single Cre-mediated recombination step to activate mutant Kras expression and do not allow genetic modeling and manipulation of sequential multistep tumorigenesis and tumor heterogeneity, which are important hallmarks of the disease. A single-step approach does not enable genetic validation of possible targets by blocking PanIN progression or treating established PDAC, nor does it enable genetic investigation of resistance mechanisms or manipulation of the tumor microenvironment.

We addressed these limitations by generating a ‘next-generation’ mouse model that allows controlled independent or sequential manipulation of genes involved in the development and maintenance of PDAC.

# RESULTS

## Sequential genetic manipulation of the pancreas

To create a dual-recombinase system (DRS), we generated transgenic mice expressing Flprecombinase directed by the mouse *Pdx1* promoter[15] (*Pdx1-Flp*; **Supplementary Fig. 1a,b**). A Flp-activated alkaline phosphatase reporter allele (*FSF-R26*$^{hpAP/+}$) revealed recombination in pancreatic islets, ducts and acini, and we observed extra-pancreatic recombination in bile duct, duodenum and stomach, paralleling established *Pdx1-Cre* lines[2,15] (**Supplementary Fig. 1c–f** and **Supplementary Table 1**).

To manipulate Flp-recombined cells sequentially using Cre, we generated a latent tamoxifen-inducible allele (*CreER*$^{T2}$) silenced by an *FRT*-stop-*FRT* (*FSF*) cassette under the control of the *CAG* promoter as a *Rosa26* knock-in (*FSF-R26*$^{CAG\text{-}CreERT2/+}$; **Supplementary Fig. 2a, b**). To activate CreER$^{T2}$ expression and monitor tamoxifen-induced CreER$^{T2}$-mediated recombination in the Flp-lineage, we used the *Pdx1-Flp* line together with a dual-fluorescent tdTomato-EGFP-Cre reporter (*R26*$^{mT\text{-}mG}$) that switches expression from tdTomato to EGFP after Cre recombination (**Supplementary Fig. 2c, d**). Tamoxifen treatment induced EGFP expression in pancreatic acini, ducts and islets; stromal cells remained unrecombined (**Supplementary Fig. 2d**). Immunohistochemistry confirmed colocalization of EGFP with markers for acini (α-amylase), ducts (CK19) and islets (insulin); we observed sporadic extrapancreatic recombination in stomach, duodenum and bile duct (**Supplementary Fig. 2c–f** and data not shown). There was no evidence of recombination in the absence of tamoxifen, excluding leaky Cre activity in this system.

## Tamoxifen-inducible genetic manipulation of the whole animal

Toxicity in non-neoplastic cells is a major limitation of many current drugs. It is thus important to evaluate the consequences of inactivating a specific therapeutic target or pathway in whole animals. To mimic drug treatment and reveal potential toxic side effects, we generated a *CreER*$^{T2}$ deleter model, *R26*$^{CAG\text{-}CreERT2}$, which ubiquitously expresses CreER$^{T2}$ (**Supplementary Fig. 3a**).

High-dose tamoxifen treatment resulted in efficient Cre recombination of the *R26*$^{mT\text{-}mG}$ reporter in various tissues, at low dose in just a few cells, whereas untreated mice showed none (**Supplementary Figs. 3b, c and 4**).

## Activation of oncogenic Kras$^{G12D}$ induces metastatic PDAC

To achieve conditional activation of oncogenic Kras in the *Pdx1-Flp* lineage, we generated a *FSF*-silenced latent *Kras*$^{G12D}$ knock-in allele (*FSF-Kras*$^{G12D/+}$; **Supplementary Fig. 5a, b**). *Kras*$^{G12D}$ expression from the endogenous promoter in *Pdx1-Flp-FSF-Kras*$^{G12D/+}$ (termed KF) mice induced PanIN precursor lesions and PDAC originating from *Pdx1-Flp*–recombined cells, as confirmed by the *FSF-R26*$^{hpAP}$ reporter (**Fig. 1a, b**).

The KF and the classical *Pdx1-Cre*;*LSL-Kras*$^{G12D/+}$ (termed KC)[2] mice showed similar patterns of PanIN progression and PDAC formation (**Fig. 1a, c, d**). Tumor latency, morphology, survival time and rates of metastasis were nearly identical (**Fig. 1d** and

**Supplementary Fig 5c–e**). PDAC in KF and KC mice were histopathologically indistinguishable, showing the full disease spectrum, from well-differentiated to undifferentiated tumors and typical liver and lung metastasis (**Fig. 1a,b**, **Supplementary Fig. 5c–e** and data not shown). Both KF and KC models thus faithfully recapitulate human PDAC[2,12].

To accelerate PDAC formation, we generated KPF mice, in which the tumor suppressor p53 is inactivated through usage of an *FRT*-flanked *Trp53* allele (*Trp53*$^{frt}$) (**Supplementary Fig. 6**). We also crossed the KF model with a mouse line that lacks p53 in the whole body (*Trp53*$^{\Delta}$) and compared PDAC formation, metastasis rates and survival with the classical KPC (*Pdx1-Cre*;*LSL-Kras*$^{G12D/+}$;*LSL-Trp53*$^{R172H/+}$) model, which carries a p53$^{R172H}$ gain of function mutation [12,16]. Again, tumors were histopathologically indistinguishable, revealing the full spectrum of human PDAC, from well- to poorly-differentiated and anaplastic tumors (**Supplementary Fig. 6a–c**). Median survival times and rates of metastasis were very similar (**Supplementary Fig. 6a–e**), and the number of metastatic lesions varied between one and several dozen in all models.

To assess extrapancreatic tumor development, we analyzed KF mice and observed sporadic noninvasive skin and bile duct papillomas and serrated duodenal adenomas in <10% of KF mice (**Fig. 1e**); by contrast, the incidence of skin papillomas is as high as 80% in KC mice[2]. Notably, we observed no extrapancreatic invasive carcinomas. Overall, the extrapancreatic pathologies of KF mice resembled those of the KC model[2] but occurred at much lower frequencies. Inactivation of p53 did not affect the frequency or invasiveness of extrapancreatic tumors, probably owing to the rapidity of PDAC development (**Supplementary Fig. 6a–c**).

These results indicate that the KF and KPF models phenocopy the widely used KC and KPC models[2,16] and may provide an improvement by reducing unwanted extrapancreatic tumor development.

## Sequential genetic manipulation of PanIN lesions and PDAC

KF mice develop PanIN and PDAC. To target and manipulate these lesions at a chosen time point using Cre-*loxP*, we crossed the *FSF-R26*$^{CAG-CreERT2}$ allele into KF mice and used the *R26*$^{mT-mG}$-Cre reporter to visualize the secondary genetic alteration (**Fig. 2a**). Tamoxifen-activation of CreER$^{T2}$ resulted in efficient excision of tdTomato and induction of EGFP in PanIN lesions *in vivo* (**Fig. 2b**). Tumor stroma showed no evidence of recombination. No recombination was detected in vehicle-treated mice (**Fig. 2b** and data not shown), excluding leaky Cre activity or spontaneous recombination events in this system.

To investigate whether our model provides the opportunity to recapitulate crucial aspects of human multistep carcinogenesis, we uncoupled temporal activation of oncogenic Kras from elimination of p53. We activated CreER$^{T2}$ by tamoxifen treatment in 2-month-old *Pdx1-Flp*;*FSF-Kras*$^{G12D/+}$;*FSF-R26*$^{CAG-CreERT2/+}$ mice with and without *loxP*-flanked (floxed) *Trp53* (**Fig. 2c,d**) and analyzed tumor development 1 month later. Inactivation of p53 in a stage-specific fashion induced rapid formation of multifocal PDAC. Histopathology revealed tumors that were well-to-moderately differentiated or undifferentiated. Untreated

*Pdx1-Flp*;*FSF-Kras*$^{G12D/+}$;*FSF-R26*$^{CAG\text{-}CreERT2/+}$;*Trp53*$^{lox/lox}$ littermate controls and tamoxifen-treated mice lacking the floxed *Trp53* showed only PanIN lesions (**Fig. 2d** and **Supplementary Fig. 7b**).

To investigate whether gene expression can be modulated in a stage-specific manner, including in established PDAC, we used a Cre-activatable *lacZ* reporter line (*LSL-R26*$^{Tva\text{-}i\text{-}lacZ}$)[4]. CreER$^{T2}$ activation by tamoxifen resulted in *lacZ* expression in PanIN and PDAC *in vivo* (**Fig. 2e** and **Supplementary Fig. 8a–c**). Again, the tumor stroma showed no apparent recombination events. Importantly, we observed no difference in recombination efficacy between stroma-rich, well-differentiated tumors and undifferentiated PDAC lacking desmoplasia (**Fig. 2e** and **Supplementary Fig. 8c**).

To manipulate PDAC *in vitro*, we isolated and cultured tumor cells from tamoxifen-naive *Pdx1-Flp*;*FSF-Kras*$^{G12D/+}$;*FSF-R26*$^{CAG\text{-}CreERT2}$ mice carrying the *R26*$^{mT\text{-}mG}$-Cre reporter. Administration of tamoxifen resulted in EGFP expression within 24 h (**Supplementary Fig. 8d**).

## The DRS enables validation of therapeutic targets

To test whether the DRS can be used to define and validate therapeutic targets *in vivo*, we crossed *Pdx1-Flp*;*FSF-Kras*$^{G12D/+}$;*FSF-R26*$^{CAG\text{-}CreERT2/+}$ mice with conditional floxed *Pdpk1* (encoding 3-phosphoinositide-dependent protein kinase 1 (Pdpk1)) knockout mice[17]. This enables tamoxifen-mediated deletion of *Pdpk1* in Kras$^{G12D}$-induced PanIN (**Fig. 3a,b**). Pdpk1 is an important downstream effector of phosphoinositide 3-kinase and essential for Kras$^{G12D}$-induced PDAC initiation[17]. However, it remains unclear whether Pdpk1 is also necessary for PDAC progression. To inactivate floxed *Pdpk1* (*Pdpk1*$^{lox/lox}$) in a time- and stage-controlled fashion after PanIN formation, we activated CreER$^{T2}$ in 3-month-old *Pdx1-Flp*;*FSFKras*$^{G12D/+}$;*FSF-R26*$^{CAG\text{-}CreERT2}$;*Pdpk1*$^{lox/lox}$ conditional knockout animals and *Pdx1-Flp*;*FSFKras*$^{G12D/+}$;*FSF-R26*$^{CAG\text{-}CreERT2}$;*Pdpk1*$^{lox/+}$ controls and analyzed pancreata in mice at age 9 months. Inactivation of both *Pdpk1* alleles resulted in macroscopically normal pancreata with normal size and weight, whereas tamoxifen-treated heterozygous *Pdpk1*$^{lox/+}$ controls showed increased pancreatic weight and size and macroscopic signs of tumor development (**Fig. 3b**). *Pdpk1*-deleted mice retained normal pancreatic tissue architecture and showed only sporadic PanINs, whereas pancreata from control mice were nearly completely replaced by tumorous tissue owing to induction of low- and high-grade PanIN lesions (**Fig. 3c,d**). Thus, *Pdpk1* ablation in PanIN-bearing animals blocked tumor progression almost completely. Notably, the few PanINs that were present in tamoxifen-treated *Pdpk1*$^{lox/lox}$ mice expressed Pdpk1 (**Fig. 3c**), suggesting incomplete recombination of the *Pdpk1* locus. This was confirmed by laser-capture microdissection and genotyping PCR, which showed the intact floxed *Pdpk1* band (**Fig. 3e**). Thus, Kras$^{G12D}$-driven PDAC progression depends on intact Pdpk1 expression.

To investigate whether the DRS can be used to validate therapeutic targets in established invasive PDAC *in vitro* and *in vivo*, we crossed *Pdx1-Flp*;*FSF-Kras*$^{G12D/+}$;*FSFR26*$^{CAG\text{-}CreERT2}$ mice with conditional *LSL-R26*$^{DTA/+}$ mice, which carry a

latent *DTA* allele (encoding diphtheria toxin A) (**Fig. 3f**). This enables depletion of all Flp-recombined cells as a proof of concept.

Tamoxifen-mediated Cre activation and DTA expression in cultured PDAC cells led to extensive cell death and depletion of PDAC cells *in vitro* (**Supplementary Fig. 9a–c**). To investigate the feasibility of PDAC depletion *in vivo*, we monitored PDAC formation in *Pdx1-Flp*;*FSF-Kras*$^{G12D/+}$;*FSF-R26*$^{CAG\text{-}CreERT2}$ mice with (DTA) or without (control) the *LSLR26*$^{DTA}$ allele by high-resolution ultrasound. Mice with established tumors of comparable size were then enrolled and treated with tamoxifen to activate Cre and express DTA. Tamoxifen-mediated DTA induction led to rapid regression of tumor volume, whereas control mice showed rapid disease progression (**Fig. 3f–h** and **Supplementary Fig. 9d**).

After 7–14 d tamoxifen treatment, mice in the conditional DTA cohort showed tumor regression, and pancreatic masses were rarely detectable by ultrasound, macroscopic pathological examination or histopathology (**Fig. 3g–j** and **Supplementary Fig. 9d–f**). Other pancreata of the DTA cohort displayed some residual small tumor nodules, with histopathological signs of intact tumor tissue (**Supplementary Fig. 9e,f**). As we expected, tamoxifen treatment resulted in pancreatitis and pancreatic atrophy due to DTA-mediated cell depletion of both neoplastic and normal pancreatic tissue (**Fig. 3i,j** and **Supplementary Fig. 9e,f**). Histopathological analysis and abnormally elevated serum lipase concentrations of tamoxifen-treated *Pdx1-Flp*;*FSF-R26*$^{CAG\text{-}CreERT2}$;*LSL-R26*$^{DTA}$ mice without the oncogenic *Kras*$^{G12D}$ allele confirmed pancreatitis induction by DTA expression. Tamoxifen-treated control mice showed normal pancreatic histology, no signs of inflammation or atrophy and normal serum lipase levels (**Supplementary Fig. 9g,h**).

To investigate whether tamoxifen or activation of CreER$^{T2}$ itself affects PDAC growth, we also treated *Pdx1-Flp*;*FSF-Kras*$^{G12D/+}$;*FSF-R26*$^{CAG\text{-}CreERT2}$ tumor cells and mice with the *FSF-R26*$^{CAG\text{-}CreERT2}$ allele but not the latent *DTA* allele with tamoxifen. These cells and tumors continued to grow after treatment (**Fig. 3g,h** and **Supplementary Fig. 9b,c**). The effects thus depend on DTA expression and not Cre recombinase toxicity[18].

## Functional analysis of cell populations within the tumor microenvironment — mast cells are dispensable for PDAC initiation.]

Mast cells link the innate and adaptive immune systems and have been implicated in tumor initiation, progression and metastasis of various tumor entities[19]. Our data show mast cell infiltration in human PDAC and in KC mice (**Supplementary Fig. 10a–e**). However, the pro- or antitumorigenic function of mast cells is controversial[20–22].

We used the DRS method to evaluate the contribution of mast cells to pancreatic carcinogenesis. To deplete mast cells *in vivo*, we used the mast cell–deficient *Cpa3*$^{Cre/+}$ line, which is not based on Kit hypomorphism[23]. This line lacks both connective tissue and mucosal mast cells owing to Cre-mediated eradication of the entire mast cell lineage. In addition to mast cells, carboxypeptidase A3 (Cpa3) is weakly expressed in hematopoietic progenitors and splenic basophils[23].

We verified mast cell deficiency in skin and pancreas of *Cpa3*$^{Cre/+}$, as compared to wild-type mice (**Fig. 4a,b**). We then analyzed mast cell infiltration and PanIN/PDAC formation in KF mice with and without *Cpa3*$^{Cre/+}$ **(Fig. 4c-g).** Staining with toluidine blue and immunofluorescent staining of the high affinity IgE receptor FcεRI revealed the absence of mast cells in PanIN and PDAC lesions of *Pdx1-Flp*;*FSF-Kras*$^{G12D/+}$;*Cpa3*$^{Cre}$ mice, whereas KF controls frequently showed mast cell infiltration (**Fig. 4c,d,f,g**). To investigate the role of mast cells in PDAC initiation, we analyzed mice deficient and proficient in mast cells at 9 months old, when all grades of PanIN are present in the KF model (**Figs. 1c** and **4e**). The number and grade of PanIN were the same, regardless of the presence of mast cells (**Fig. 4e**). We also analyzed some mice at age 12 months. These showed sporadic occurrence of invasive PDAC, again regardless of whether mast cells were present (**Fig. 4f,g**).

Mast cells are therefore dispensable for PDAC formation. Previous reports have, however, described dramatically altered tumor development and growth in mast cell–deficient hypomorphic *Kit*-mutant mice (e.g. *Kit*$^{W\text{-}sh}$), or mice treated with cromolyn, a mast cell stabilizer[20,24,25]. We investigated expression of the *Kit* proto-oncogene during pancreatic carcinogenesis and frequently observed Kit expression in PanIN and PDAC cells by immunohistochemistry (**Supplementary Fig. 10f,g**). Kit expression in pancreas was also analyzed by lineage tracing with a tamoxifen-inducible *Kit*$^{CreERT2}$ knock-in mouse line[26], revealing that Kit marks a distinct pancreatic cell population (**Supplementary Fig. 10h**). The *R26*$^{mT\text{-}mG}$-Cre reporter indicated no leaky Cre activity in the absence of tamoxifen.

These data indicate that hypomorphic *Kit* mutations may contribute to the altered tumor phenotype of mast cell–deficient models in a mast cell–independent manner[23].

To gain insight into gene expression changes associated with mast cell deficiency, we performed mRNA expression profiling of pancreatic tumors and obtained a statistically significant gene expression signature of mast cell deficiency in *Pdx1-Flp*;*FSF Kras*$^{G12D/+}$;*Cpa3*$^{Cre/+}$ mice using “gene set enrichment analysis” (GSEA) (Normalized Enrichment Score: -1.5837048; Nominal *P*-value: 0.008152174; False Discovery Rate (FDR) *q*-value: 0.0096; see also **Supplementary Results**). mRNA expression analysis of genes relevant to PDAC revealed no significant ($P < 0.05$) changes due to mast cell ablation, except for C-X-C motif chemokine 13 (Cxcl13), fibroblast growth factor 21 (Fgf21) and interleukin 2 receptor gamma (Il2rg) (**Supplementary Fig. 11a,b** and data not shown). Only 155 probe sets (0.44%), corresponding to 108 annotated genes, showed significantly ($P < 0.05$) different changes (>2-fold) in mRNA expression between mast cell deficient and proficient pancreatic tumors (**Supplementary Fig. 11c**). In addition to the aforementioned three gene products, cathepsin E and the mucin Muc5ac have been linked to pancreatic disease (**Supplementary Fig. 11d**). Thus, cancer-relevant pathways are not broadly affected by mast cell deficiency, corroborating our finding that mast cells do not influence PDAC development.

## DISCUSSION

Breakthroughs in cancer research, such as genomic analysis and high-throughput drug and genetic screening, are providing a wealth of resources and large, complex data sets.

Understanding and interpreting the biological and clinical relevance of these resources is a significant challenge but holds the promise of breakthrough treatments for particularly difficult conditions, such as PDAC.

What has so far made it difficult to take full advantage of these developments is a means of realistically modeling and manipulating the developing tumor entity and its microenvironment. This is vital for the identification and assessment of candidate therapeutic targets. We have generated, characterized and validated a next-generation DRS that enables sequential genetic manipulation of PanIN and PDAC cells and the host on a genome-wide scale *in vivo*. Combining the Flp-*FRT* recombination system for tumor initiation with the 'universal' Cre-*loxP* system for secondary genetic manipulation provides researchers with new opportunities to model, manipulate and investigate diverse aspects of malignant tumors in whole animals. This includes rigorous genetic analysis of (i) genetic alterations in multistep carcinogenesis, (ii) tumor cell subpopulations such as cancer stem cells, (iii) the tumor microenvironment, (iv) immune cell subpopulations, (v) the metastatic niche of host organs, (vi) therapeutic targets and (vii) resistance mechanisms (**Fig. 5**).

The PDAC stroma supports tumor growth and mediates drug resistance and is clearly relevant to future therapies[12,14]. It is therefore important to understand the biology of the different stromal subcomponents. To demonstrate the utility of the DRS-based PDAC model as a means of targeting the tumor microenvironment, we investigated the role of mast cells and showed that they are dispensable for PDAC initiation and progression (**Supplementary Results**).

Besides evaluating stromal subpopulations, the DRS-based PDAC model enables sequential mutagenesis within tumor-initiating cells or precursor PanIN lesions, as previously used to study p53 loss during sarcomagenesis[27]. It also allows rigorous genome-wide testing of tumor cell–intrinsic therapeutic targets. Synthetic lethal interaction partners of oncogenic Kras[28] and multiple novel candidate genes and pathways identified via genome-wide small hairpin RNA– and transposon-based forward genetic screens and next-generation sequencing[28–30] demonstrate impressively that potential treatment targets are available. These await rigorous genetic validation *in vivo*.

We demonstrated secondary genetic targeting, thus mimicking therapeutic interventions, using a floxed *Pdpk1* mouse line and a latent *DTA* allele as proof of concept. Our model thus provides an ideal complement for genome-wide mouse embryonic stem cell repositories and mutant lines with Cre-inducible somatic inactivation of every gene, enabling genome-wide target validation[31]. The synergistic power of these developments will spur the field.

Two groups have generated transgenic GEMMs that allow tetracycline (TET)-inducible expression of oncogenic Kras in pancreas and its time-specific inactivation[32,33]. These showed that continuous oncogenic Kras activity is essential for tumor maintenance[32,33]. Combined with Cre-*loxP*, Flp-*FRT* and other recombination systems such as Dre-*rox*, these TET-Kras mice, as well as novel embryonic stem cell–based PDAC models[34], will further increase the possibilities of modeling and manipulating PDAC cells and their microenvironment.

In summary, we developed a next-generation Flp-*FRT*–based spontaneous model of Kras-driven stroma-rich PDAC that recapitulates major hallmarks of human PDAC with minimal extrapancreatic disease. The use of secondary modifications allows genetic dissection of the native biology of PDAC tumors and their associated stroma and rigorous genetic validation of candidate therapeutic targets. The DRS model can thus contribute directly to the development of new therapeutic strategies. Generation of tissue-specific Flp driver lines or viral Flp delivery[27,35] will allow spatial and temporal control of gene expression in various cancer models. The DRS approach is highly versatile with wide applicability and has the potential to significantly advance cancer research.

## ONLINE METHODS

### Materials

All cell culture reagents were obtained from Invitrogen (Groningen, The Netherlands). Primers were made by MWG (Ebersberg, Germany) and restriction endonucleases obtained from New England Biolabs (Mannheim, Germany). The *E. coli* strains TOP10 and Stbl3 (Invitrogen, Groningen, The Netherlands) were used for transformation and plasmid amplification. 4-Hydroxytamoxifen (H6278) and peanut oil (P2144) were purchased from Sigma (Deisenhofen, Germany).

### Mouse strains and tumor models

*LSL-Kras*$^{G12D/+}$[2], *Pdx1-Cre*[2], *LSL-Trp53*$^{R172H/+}$[16], *Trp53*$^{frt/+}$[35], *Trp53*$^{lox/+}$[36], *Trp53*$^{\Delta/+}$[37], *LSL-R26*$^{Tva\text{-}i\text{-}lacZ/+}$[4], *R26*$^{mT\text{-}mG/+}$[38], *FSF-R26*$^{hpAP/+}$[39], *Pdpk1*$^{lox/+}$[40], *Cpa3*$^{Cre/+}$[23], *Kit*$^{CreERT2/+}$[26], *R26*$^{Flpo/+}$[41] and *LSL-R26*$^{DTA/+}$[42] have been described previously. Unless otherwise stated, animals were on a mixed *C57Bl/6*;*129S6/SvEv* genetic background. The strains were interbred to obtain mice with activation of oncogenic Kras$^{G12D}$ in the pancreas as previously described[10]. Age- and sex-matched randomized animals were used as indicated and no animals were excluded from analyses. All animal studies were conducted in compliance with European guidelines for the care and use of laboratory animals and were approved by the Institutional Animal Care and Use Committees (IACUC) of Technische Universität München, Regierung von Oberbayern and UK Home Office.

### Construction of the *Pdx1-Flp* transgenic line

To generate the *Pdx1-Flp* construct, a 6.3 kb fragment containing the *Pdx1* promoter from pKSpdx-1SalI (#571, a kind gift from C. Wright; see **Supplementary Figure 1a**) was ligated to the codon optimized *Flp-o* cDNA (a kind gift from P. Soriano; Addgene plasmid # 13792;[41]). The start codon of the *Flp-o* cDNA was directly fused to the ATG start codon of the *Pdx1* gene. The human beta globin polyadenylation signal sequence was ligated 3’ of the *Flp-o* expression construct. The 8.1 kb insert was released from pBluescript by SalI-PmeI digestion and was used for pronuclear injection into *C57BL/6* zygotes (Polygene, Rümlach, Switzerland).

## Construction of targeting vectors and generation of *FSF-R26$^{CAG\text{-}CreERT2}$* and *FSF Kras$^{G12D}$* knock-in mouse lines

*Rosa26* targeting by a knock-in strategy was performed on the basis of plasmid *pROSA26–1* as previously described[4]. A targeting vector containing a *CAG* promoter and a *FRT*-flanked transcriptional and translational stop cassette (*FRT*-stop-*FRT*; FSF) with a neomycin resistance gene 5' of the *CreER$^{T2}$* expression cassette was generated by standard cloning procedures (**Supplementary Figure 2a**). The targeting vector was linearized and electroporated into *129S6/SvEv* embryonic stem (ES) cells. Cells were selected with 200 μg ml$^{-1}$ Geneticin, and correctly targeted homologous recombined clones identified by PCR as described[4]. Correct recombination and single copy insertion was verified by long range and quantitative PCR, respectively. Germ-line transmission was achieved in 2/2 clones harboring the targeted allele. A three-primer PCR strategy (**Supplementary Figure 2b**) was used to genotype *FSF-R26$^{CAG\text{-}CreERT2}$* animals as described[4].

To generate a novel tamoxifen-inducible *CreER$^{T2}$* deleter mouse line (termed *R26$^{CAG\text{-}CreERT2}$*), which ubiquitously expresses CreER$^{T2}$, we deleted the *FRT*-flanked transcriptional stop cassette in *FSF-R26$^{CAG\text{-}CreERT2}$* animals using the *R26$^{Flpo/+41}$* deleter line.

To construct the *FSF-Kras$^{G12D}$* targeting vector, we used a *Kras* genomic clone, amplified the long and short arm of the *Kras* targeting vector by PCR and introduced a codon 12 aspartic acid mutation into exon 2 by site-directed mutagenesis. Finally, a FSF cassette with a splice acceptor 3' of the first *FRT* recombination site and a promoterless *neomycin* resistance cassette was introduced into the first intron of the *Kras* targeting vector (**Supplementary Figure 5a**). All constructs were verified by sequencing. We electroporated the *PacI* linearized targeting vector into *129S6/SvEv* ES cells and selected appropriately targeted clones with 200 μg ml$^{-1}$ Geneticin. Homologous recombined clones were identified by PCR and correct recombination and single copy insertion was verified by long range PCR and quantitative PCR, respectively. Two clones were injected into blastocysts (Polygene, Rümlach, Switzerland). Germ-line transmission was achieved in 2/2 clones harboring the targeted allele. A three-primer PCR strategy (**Supplementary Figure 5b**) was used to genotype animals.

## Fluorescence stereomicroscopy and quantification of metastasis frequency

Macroscopic analysis of mouse tissues, PDAC and metastases was performed using a Zeiss Stemi 11 fluorescence stereomicroscope. At necropsy, all abdominal organs and the lungs were investigated macroscopically for metastases as described[17,43]. For microscopic quantification of metastases at least three series of sections (100 μm between the different series) of paraffin embedded lungs and livers of 20 mice per genotype with PDAC were prepared, H&E stained and investigated for the presence of metastases by an examiner blinded to the genotype of the animals.

## Fluorescence *in situ* hybridization (FISH)

Metaphase spreads were prepared from splenocytes using standard protocols and fluorescence *in situ* hybridization was performed as described[44]. Probes specific for the *Flp*

transgene were amplified using GenomePlex® Complete Whole Genome Amplification (WGA) kit (WGA2, Sigma) and labeled directly with ChromaTide Texas Red dUTP (Invitrogen) using GenomePlex® WGA Reamplification Kit (WGA3, Sigma) and custom-made dNTP mixture. Probes were then denatured for 10 min at 65 °C and preannealed for approximately 30 – 45 min at 37 °C. Slides were prepared one week in advance, to age metaphases at RT with a desiccant. Slides were then pretreated in prewarmed 2 × SSC and pepsin (75 μl of 1% pepsin in 50 ml of 0.01 M HCl) at 37 °C for 5 min each. Slides were washed 3 times in 2 × SSC for 3 min, and then treated for 10 min in formaldehyde fixative (1.25 ml of formaldehyde, 40% w/v and 2.5 ml of 1 M $MgCl_2$, 50 mM $MgCl_2$ in PBS) at RT. Slides were washed 3 times in 2 × SSC for 3 min, passed through an ethanol series and air dried. Slides were then denatured in 70% formamide, 2 × SSC for 1 min 30 s, at 63 °C and passed again through an ethanol series and air dried. Denatured preannealed probes were added to the slides, covered with coverslips, sealed with Fixogum rubber cement (Marabu) and incubated overnight at 37 °C. To remove unbound probes, slides were subjected to post-hybridization washes and mounted in SlowFade (Invitrogen) with DAPI (4,6 diamidino-2-phenylindole), overlayed with coverslip and sealed with nail varnish. Metaphases were scanned using an epifluorescence microscope equipped with a CCD camera and narrow band-pass filters. Images were captured using the SmartCapture software (Digital Scientific, UK) and metaphases were karyotyped using the SmartType Karyotyper software (Digital Scientific).

### Generation and culture of primary mouse PDAC cell lines

Primary dispersed mouse pancreatic cancer cells were established and cultivated as previously described[43]. PDAC cells were cultured in DMEM supplemented with 10% FCS and 0.1 or 0.5 μM 4-hydroxytamoxifen or vehicle (ethanol) to delete *loxP* flanked sequences *in vitro*. Cell proliferation was quantified by cell counting on consecutive days. All cell lines were authenticated by genotyping and tested for mycoplasma contamination.

### Tamoxifen treatment of mice

Mice were fed with tamoxifen-containing chow (400 mg tamoxifen citrate $kg^{-1}$ chow; CreActive TAM400, LASvendi, Soest, Germany) for 2 or 4 weeks to activate $CreER^{T2}$.

### High-resolution ultrasound

Mice were screened for tumors by abdominal palpation. Palpable tumors were verified by high-resolution ultrasound (Vevo 2100, VisualSonics). Animals with average tumor diameters greater than 5 mm were enrolled in the treatment study as described[17]. Tumor volumes were determined by automated three-dimensional (3D) B-mode imaging along the entire length of the tumor (VisualSonics). Reconstructed three-dimensional ultrasound imaging data sets were analyzed and tumor volumes were quantified using the integrated Vevo 2100 software package (VisualSonics) by an examiner blinded to the genotype of the animals. Macroscopic tumor perfusion was analyzed using the Doppler mode of the Vevo 2100 system.

### Quantitative reverse-transcriptase PCR

Total RNA was isolated from tissues using the RNeasy kit (Qiagen, Hilden, Germany) following the manufacturer's instructions and reverse transcribed (Invitrogen). Quantitative mRNA analyses were performed using real-time PCR analysis (TaqMan, PE Applied Biosystems, Norwalk, CT) and QuantiTect Primer Assays (Qiagen) as previously described[45].

### Laser capture microdissection and DNA extraction

PanIN lesions and normal acini from 8 μm thick, dewaxed, hematoxylin and eosin stained formalin fixed paraffin embedded tissue sections were microdissected using a P.A.L.M. laser capture microdissection system (Zeiss, Göttingen, Germany) as described previously[46]. DNA was isolated from the microdissected cells using the QIAamp DNA Micro Kit (Qiagen, Hilden, Germany).

### Histochemistry and immunohistochemistry

For histopathology, mouse tissue specimens were fixed in 4% buffered formalin overnight, embedded in paraffin and sectioned (2.5 μm thick). Quantification and grading of mouse ADM and PanIN lesions was performed on three sections per mouse and 3 mice per time point according to the established nomenclature for the grading of PanIN lesions in mice[47]. The examiner was blinded to the genotype of the animals. Alcian blue staining was performed on paraffin embedded tissue sections using aqueous alcian blue solution (pH 2.5). Sections were counterstained with nuclear fast red, as previously described[17]. Toluidine blue staining of mast cells was performed using an aqueous toluidine blue staining solution (pH 2.0) for 10 min (all staining solutions from Sigma). For immunodetection, formalin-fixed paraffin-embedded tissue sections were dewaxed, rehydrated and placed in a microwave (10 min, 600 watt) to recover antigens. Sections were incubated with primary c-Kit (C-19; sc-168; 1:50; Santa Cruz Biotechnology, Santa Cruz, CA), p53 (NCL-p53-CM5p; rabbit, 1:400; Novocastra/Leica Mikrosysteme, Wetzlar, Germany) and Pdpk1 (Pdk1, #3061; rabbit, 1:50; Cell Signaling Technology, Danvers, MA) antibodies followed by a secondary antibody conjugated to biotin (Vector Laboratories, Burlingame, CA).

### β-galactosidase staining

β-galactosidase staining of cryosections was performed as described previously[4]. Counterstaining was carried out with eosin or nuclear fast red.

### Alkaline phosphatase (AP) staining

Cryosections were post-fixed in 4% paraformaldehyde in PBS for 10 min at 4 °C. After rinsing with cold PBS, sections were incubated at 70 °C in preheated PBS for 30 min, followed by incubation in AP detection buffer (100 mM NaCl, 100 mM Tris-HCl pH 9.5, 50 mM $MgCl_2$) for 30 min. Sections were subsequently placed in AP staining solution (AP detection buffer with 0.8 mg $ml^{-1}$ nitroblue tetrazolium (NBT), 0.1 mg $ml^{-1}$ 5-bromo-4-chloro-3-indolyl phosphate dimethylformamide (BCIP), 0.01% sodium deoxycholate, 0.02% NP-40, and 0.5 mM levamisole) at room temperature overnight. Once color development was complete, sections were counterstained with nuclear fast red or eosin.

### Immunofluorescence staining

Mouse tissues were fixed in 4% buffered formalin for 2 h, dehydrated in sucrose solution at 4 °C (15% sucrose in PBS for 4 h; 30% sucrose in PBS overnight) and embedded in Tissue-Tek® (Sakura, Torrance, CA) before being rapidly frozen in liquid nitrogen. 20 μm thick frozen sections were post-fixed for 1 min in 4% buffered formalin, washed twice in PBS and incubated for 1 h in PBS with 3% (w/v) bovine serum albumin (BSA), 1% (w/v) Saponin and 1% (v/v) Triton-X 100. Subsequently, slides were incubated for 48 h at 4 °C in the dark with primary antibodies: Kit (M14; goat, 1:100; sc-1494, Santa Cruz Biotechnology, Santa Cruz, CA), alpha-amylase (A8273; rabbit, 1:100; Sigma-Aldrich), insulin (C27C9; rabbit, 1:100; #3014, Cell Signaling Technology), CK19 (ab52625; rabbit, 1:75; abcam, Cambridge, UK), or PE labeled FcεRI alpha (#12-5898-82; hamster, 1:100; eBioscience, Frankfurt, Germany) as described[26]. Kit, α-amylase, insulin and CK19 antibody stained slides were incubated in the dark with secondary antibody Alexa Fluor® 488 donkey anti-goat (1:100, Invitrogen), DyLight® 680 goat anti-rabbit IgG (H+L) (1:100; #5366), or DyLight® 800 goat anti-rabbit IgG (H+L) (1:100; #5151, both from Cell Signaling Technology). Nuclei were counterstained in selected sections with TOPRO®-3-iodide (1:1000, Invitrogen) for 2 h at RT. Selected sections were additionally counterstained with Alexa Fluor® 594 labeled phalloidin (1:250, Invitrogen) to visualize actin filaments and thus cell morphology. After three rinses in PBS, slides were mounted with Vectashield Mounting Medium (Vector Laboratories, Burlingame, CA).

### Confocal laser-scanning microscopy

Cryosections were examined by confocal laser scanning confocal microscopy (LSM) with a Zeiss LSM 510 Axiovert 100 microscope (Zeiss, Oberkochen, Germany) with a ×20/0.5 air and a ×40/1.3 oil-immersion objective (optical section thickness 4.4 mm) as described[26]. Images (single optical sections and z-stacks, z-step size 0.5 mm) with a frame size of 1,024 × 1,024 pixels and an image size of 225 × 225 mm (×40/1.3 objective, Zeiss), or 450 × 450 mm (×20/0.5 air objective, Zeiss) were collected. Images were merged and converted with Zeiss LSM 510 software.

### Staining and counting of skin mast cells

Staining of skin mast cells was performed as described[26]. In brief, ears of the respective animals were separated into a ventral and dorsal half and fixed in 1% buffered formalin overnight at 4 °C. After incubation for 1 h at RT in 1% BSA in PBS, mast cells were stained with avidin-Texas Red (1:500, Invitrogen) as described[26]. Nuclei were counterstained with TOPRO®-3-iodide. For mast cell-counting, the ears of at least 3 mice per genotype and 10 – 15 fields of view of each animal were analysed by LSM using the Zeiss LSM 510 microscope with a × 20/0.5 air objective. The examiner was blinded to the genotype of the animals.

### RNA expression analyses

RNA extraction and microarray expression analyses were performed as recently described[43,48]. In brief, total RNA was prepared using RNeasy Kit (Qiagen) and processed with the Ambion WT expression kit (Applied Biosystems). Purified single-stranded cRNA

was fragmented and labeled by using the GeneChip WT terminal labeling kit (Affymetrix, Santa Clara, CA) and hybridized onto Affymetrix GeneChip Mouse Gene 1.0 ST Array. Calculation of expression values was done by taking the mean of all perfect match probes for each probeset. The expression dataset was quantile normalized and each probeset was assessed for differential expression with standard Student's *t* test. Resulting *P*-values are corrected for the number of tests (48107) with the method by Benjamini & Hochberg[49]. Gene set enrichment analysis (GSEA) was performed with GSEA software (Broad Institute, MIT, MA; www.broadinstitute.org)[50]. Genes down-regulated > 2 fold in mast cell-deficient tissues (peritoneum and ear)[23] were defined as gene set "Mast_cell_deficiency". *P*-values < 0.05 with a false discovery rate (FDR) *q*-value < 0.05 (5%) and a family-wise error rate (FWER) *P*-value < 0.05 were considered to be statistically significant. Heatmaps for the expression levels of selected genes were assembled with the GenePattern software package (Broad Institute). Microarray data are available in the EMBLEBI ArrayExpress database (www.ebi.ac.uk/arrayexpress) under accession number E-MTAB-2551.

### Data analysis

Unless otherwise indicated, all data were determined from at least three independent experiments and expressed as mean values ± s.e.m. Sample size was calculated using GraphPad StatMateSoftware 2.00 (GraphPad Software, Inc.; La Jolla, CA). Statistical comparisons between data sets were made with analysis of normality and variance, followed by a two-sided unpaired Student's *t* test. A Bonferroni correction of the *P* values was performed for pair wise multiple testing. Fisher's exact test was performed by using STATXACT 4.0.1 software (Cytel Software, Cambridge, MA) as described[51]. Values of $P < 0.05$ were considered to be statistically significant.

## Supplementary Material

Refer to Web version on PubMed Central for supplementary material.

## ACKNOWLEDGMENTS

The authors thank A. Berns (Netherlands Cancer Institute), S. Dymecki (Harvard Medical School), T. Jacks (Massachusetts Institute of Technology), L. Luo (Stanford University), J. Martinez-Barbera (University College London) and D. Tuveson (Cold Spring Harbor Laboratory) for providing transgenic animals, C. Wright (Vanderbilt University) for the mouse *Pdx1* promoter construct, P. Soriano (Mount Sinai School of Medicine) for the Flp-o expression vector and the *R26* targeting vector, T. Schmidt and M. Bewerunge-Hudler (DKFZ Microarray Core Facility) for mRNA analyses, and J. Götzfried, U. Götz and S. Jaeckel for technical assistance. This work was supported by funding from Deutsche Forschungsgemeinschaft (DFG SA 1374/4-1 to D.S. and SFB824, TP C9 to G.S. and D.S.), the Helmholtz Alliance Preclinical Comprehensive Cancer Center (to H.R.R., R.R., R.M.S. and D.S.), the German Cancer Consortium (DKTK) (to R.R., R.M.S. and D.S.), the Wilhelm-Sander Foundation (2012.084.1 to G.S.), the Spanish Ministerio de Economía y Competitividad subprograma Ramón y Cajal (I.V.), the European Union (ERC Advanced Grant No.233074 to H.R.R.), and the National Cancer Institute USA (R01 CA138265 to D.G.K. and CA155620 to A.M.L.).

## References

1. Siegel R, Naishadham D, Jemal A. Cancer statistics, 2013. CA Cancer J. Clin. 2013; 63:11–30. [PubMed: 23335087]
2. Hingorani SR, et al. Preinvasive and invasive ductal pancreatic cancer and its early detection in the mouse. Cancer Cell. 2003; 4:437–450. [PubMed: 14706336]

3. Guerra C, et al. Chronic pancreatitis is essential for induction of pancreatic ductal adenocarcinoma by K-Ras oncogenes in adult mice. Cancer Cell. 2007; 11:291–302. [PubMed: 17349585]
4. Seidler B, et al. A Cre-loxP-based mouse model for conditional somatic gene expression and knockdown in vivo by using avian retroviral vectors. Proc. Natl. Acad. Sci. USA. 2008; 105:10137–10142. [PubMed: 18621715]
5. Pylayeva-Gupta Y, Grabocka E, Bar-Sagi D. RAS oncogenes: weaving a tumorigenic web. Nat. Rev. Cancer. 2011; 11:761–774. [PubMed: 21993244]
6. Carrière C, Seeley ES, Goetze T, Longnecker DS, Korc M. The Nestin progenitor lineage is the compartment of origin for pancreatic intraepithelial neoplasia. Proc. Natl. Acad. Sci. USA. 2007; 104:4437–4442. [PubMed: 17360542]
7. Habbe N, et al. Spontaneous induction of murine pancreatic intraepithelial neoplasia (mPanIN) by acinar cell targeting of oncogenic Kras in adult mice. Proc. Natl. Acad. Sci. USA. 2008; 105:18913–18918. [PubMed: 19028870]
8. Gidekel Friedlander SY, et al. Context-dependent transformation of adult pancreatic cells by oncogenic K-Ras. Cancer Cell. 2009; 16:379–389. [PubMed: 19878870]
9. Morris, J.P.t.; Wang, SC.; Hebrok, M. KRAS, Hedgehog, Wnt and the twisted developmental biology of pancreatic ductal adenocarcinoma. Nat. Rev. Cancer. 2010; 10:683–695. [PubMed: 20814421]
10. Eser S, et al. In vivo diagnosis of murine pancreatic intraepithelial neoplasia and early-stage pancreatic cancer by molecular imaging. Proc. Natl. Acad. Sci. USA. 2011; 108:9945–9950. [PubMed: 21628592]
11. Mazur PK, Siveke JT. Genetically engineered mouse models of pancreatic cancer: unravelling tumour biology and progressing translational oncology. Gut. 2012; 61:1488–1500. [PubMed: 21873467]
12. Olive KP, et al. Inhibition of Hedgehog signaling enhances delivery of chemotherapy in a mouse model of pancreatic cancer. Science. 2009; 324:1457–1461. [PubMed: 19460966]
13. Pylayeva-Gupta Y, Lee KE, Hajdu CH, Miller G, Bar-Sagi D. Oncogenic Kras-induced GM-CSF production promotes the development of pancreatic neoplasia. Cancer Cell. 2012; 21:836–847. [PubMed: 22698407]
14. Provenzano PP, et al. Enzymatic targeting of the stroma ablates physical barriers to treatment of pancreatic ductal adenocarcinoma. Cancer Cell. 2012; 21:418–429. [PubMed: 22439937]
15. Gannon M, Herrera PL, Wright CV. Mosaic Cre-mediated recombination in pancreas using the pdx-1 enhancer/promoter. Genesis. 2000; 26:143–144. [PubMed: 10686611]
16. Hingorani SR, et al. Trp53R172H and KrasG12D cooperate to promote chromosomal instability and widely metastatic pancreatic ductal adenocarcinoma in mice. Cancer Cell. 2005; 7:469–483. [PubMed: 15894267]
17. Eser S, et al. Selective requirement of PI3K/PDK1 signaling for Kras oncogene-driven pancreatic cell plasticity and cancer. Cancer Cell. 2013; 23:406–420. [PubMed: 23453624]
18. Schmidt-Supprian M, Rajewsky K. Vagaries of conditional gene targeting. Nat. Immunol. 2007; 8:665–668. [PubMed: 17579640]
19. Theoharides TC, Conti P. Mast cells: the Jekyll and Hyde of tumor growth. Trends Immunol. 2004; 25:235–241. [PubMed: 15099563]
20. Theoharides TC. Mast cells and pancreatic cancer. N. Engl. J. Med. 2008; 358:1860–1861. [PubMed: 18434656]
21. Nielsen HJ, et al. Independent prognostic value of eosinophil and mast cell infiltration in colorectal cancer tissue. J. Pathol. 1999; 189:487–495. [PubMed: 10629548]
22. Rajput AB, et al. Stromal mast cells in invasive breast cancer are a marker of favourable prognosis: a study of 4,444 cases. Breast Cancer Res. Treat. 2008; 107:249–257. [PubMed: 17431762]
23. Feyerabend TB, et al. Cre-mediated cell ablation contests mast cell contribution in models of antibody- and T cell-mediated autoimmunity. Immunity. 2011; 35:832–844. [PubMed: 22101159]
24. Soucek L, et al. Mast cells are required for angiogenesis and macroscopic expansion of Myc-induced pancreatic islet tumors. Nat. Med. 2007; 13:1211–1218. [PubMed: 17906636]

25. Chang DZ, et al. Mast cells in tumor microenvironment promotes the in vivo growth of pancreatic ductal adenocarcinoma. Clin. Cancer Res. 2011; 17:7015–7023. [PubMed: 21976550]
26. Klein S, et al. Interstitial cells of Cajal integrate excitatory and inhibitory neurotransmission with intestinal slow-wave activity. Nat. Commun. 2013; 4:1630. [PubMed: 23535651]
27. Young NP, Crowley D, Jacks T. Uncoupling cancer mutations reveals critical timing of p53 loss in sarcomagenesis. Cancer Res. 2011; 71:4040–4047. [PubMed: 21512139]
28. Luo J, et al. A genome-wide RNAi screen identifies multiple synthetic lethal interactions with the Ras oncogene. Cell. 2009; 137:835–848. [PubMed: 19490893]
29. Biankin AV, et al. Pancreatic cancer genomes reveal aberrations in axon guidance pathway genes. Nature. 2012; 491:399–405. [PubMed: 23103869]
30. Pérez-Mancera PA, et al. The deubiquitinase USP9X suppresses pancreatic ductal adenocarcinoma. Nature. 2012; 486:266–270. [PubMed: 22699621]
31. Skarnes WC, et al. A conditional knockout resource for the genome-wide study of mouse gene function. Nature. 2011; 474:337–342. [PubMed: 21677750]
32. Ying H, et al. Oncogenic Kras maintains pancreatic tumors through regulation of anabolic glucose metabolism. Cell. 2012; 149:656–670. [PubMed: 22541435]
33. Collins MA, et al. Oncogenic Kras is required for both the initiation and maintenance of pancreatic cancer in mice. J. Clin. Invest. 2012; 122:639–653. [PubMed: 22232209]
34. Saborowski M, et al. A modular and flexible ESC-based mouse model of pancreatic cancer. Genes Dev. 2014; 28:85–97. [PubMed: 24395249]
35. Lee C-L, et al. Generation of primary tumors with Flp recombinase in FRT-flanked p53 mice. Dis. Model. Mech. 2012; 5:397–402. [PubMed: 22228755]
36. Jonkers J, et al. Synergistic tumor suppressor activity of BRCA2 and p53 in a conditional mouse model for breast cancer. Nat. Genet. 2001; 29:418–425. [PubMed: 11694875]
37. Olive KP, et al. Mutant p53 gain of function in two mouse models of Li-Fraumeni syndrome. Cell. 2004; 119:847–860. [PubMed: 15607980]
38. Muzumdar MD, Tasic B, Miyamichi K, Li L, Luo L. A global double-fluorescent Cre reporter mouse. Genesis. 2007; 45:593–605. [PubMed: 17868096]
39. Awatramani R, Soriano P, Mai JJ, Dymecki S. An Flp indicator mouse expressing alkaline phosphatase from the ROSA26 locus. Nat. Genet. 2001; 29:257–259. [PubMed: 11687793]
40. Lawlor MA, et al. Essential role of PDK1 in regulating cell size and development in mice. EMBO J. 2002; 21:3728–3738. [PubMed: 12110585]
41. Raymond CS, Soriano P. High-efficiency FLP and PhiC31 site-specific recombination in mammalian cells. PLoS ONE. 2007; 2:e162. [PubMed: 17225864]
42. Ivanova A, et al. In vivo genetic ablation by Cre-mediated expression of diphtheria toxin fragment A. Genesis. 2005; 43:129–135. [PubMed: 16267821]
43. von Burstin J, et al. E-cadherin regulates metastasis of pancreatic cancer in vivo and is suppressed by a SNAIL/HDAC1/HDAC2 repressor complex. Gastroenterology. 2009; 137:361–371. 371, e361–365. [PubMed: 19362090]
44. Rad R, et al. PiggyBac transposon mutagenesis: a tool for cancer gene discovery in mice. Science. 2010; 330:1104–1107. [PubMed: 20947725]
45. Saur D, et al. CXCR4 expression increases liver and lung metastasis in a mouse model of pancreatic cancer. Gastroenterology. 2005; 129:1237–1250. [PubMed: 16230077]
46. Flisikowska T, et al. A porcine model of familial adenomatous polyposis. Gastroenterology. 2012; 143:1173–1175.e1171-1177. [PubMed: 22864254]
47. Hruban RH, et al. Pathology of genetically engineered mouse models of pancreatic exocrine cancer: consensus report and recommendations. Cancer Res. 2006; 66:95–106. [PubMed: 16397221]
48. Diersch S, et al. Efemp1 and p27(Kip1) modulate responsiveness of pancreatic cancer cells towards a dual PI3K/mTOR inhibitor in preclinical models. Oncotarget. 2013; 4:277–288. [PubMed: 23470560]
49. Benjamini Y, Hochberg Y. Controlling the False Discovery Rate: A Practical and Powerful Approach to Multiple Testing. J. R. Stat. Soc., B. 1995; 57:289–300.

50. Subramanian A, et al. Gene set enrichment analysis: a knowledge-based approach for interpreting genome-wide expression profiles. Proc. Natl. Acad. Sci. USA. 2005; 102:15545–15550. [PubMed: 16199517]

51. Saur D, et al. Single-nucleotide promoter polymorphism alters transcription of neuronal nitric oxide synthase exon 1c in infantile hypertrophic pyloric stenosis. Proc. Natl. Acad. Sci. USA. 2004; 101:1662–1667. [PubMed: 14757827]

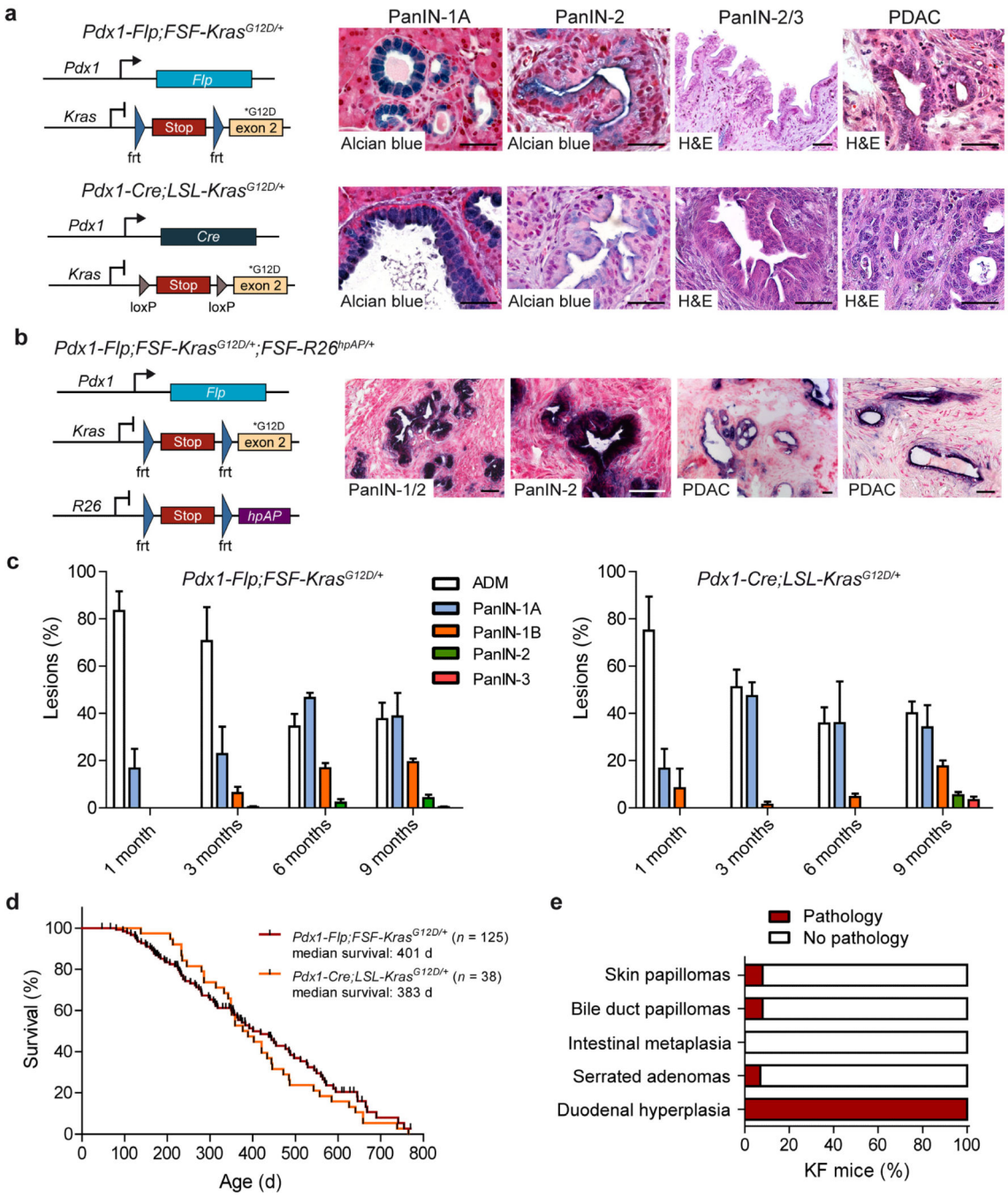


**Figure 1.**

*Pdx1-Flp*–activated expression of oncogenic Kras$^{G12D}$ induces premalignant PanIN and PDAC. (**a**) Left, genetic strategy to activate oncogenic Kras in the pancreas using the Flp-*FRT* (top) and the Cre-*loxP* (bottom) recombination system. Right, representative alcian blue and hematoxylin and eosin (H&E) stained sections of different grades (1-3) of pancreatic intraepithelial neoplasia (PanIN) and invasive PDAC of male and female *Pdx1-Flp*;*FSFKras*$^{G12D/+}$ (top) and *Pdx1-Cre*;*LSL-Kras*$^{G12D/+}$ (bottom) mice. (**b**) Genetic strategy to induce oncogenic Kras$^{G12D}$ and human placental alkaline phosphatase (hpAP)

reporter gene expression in the *Pdx1-Flp* lineage (left). Representative alkaline phosphatase staining (purple) of the indicated grades of PanIN lesions and PDAC cells in male and female *Pdx1-Flp*;*FSF-Kras*$^{G12D/+}$;*FSF-R26*$^{hpAP/+}$ mice (right). (**c**) Quantification of acinar to ductal metaplasia (ADM) and PanIN progression (from PanIN grade -1A (flat epithelial lesion), -1B (papillary lesion), -2 (lesion with nuclear abnormalities) to PanIN grade -3 (carcinoma in situ)) as a percentage of total lesions in *Pdx1-Flp*;*FSF-Kras*$^{G12D/+}$ and *Pdx1-Cre*;*LSLKras*$^{G12D/+}$ mice (error bars, s.e.m.; $n = 3$ representative slides from three mice per time point and genotype). (**d**) Kaplan-Meier survival curves of *Pdx1-Flp*;*FSF-Kras*$^{G12D/+}$ and *Pdx1-Cre*;*LSL-Kras*$^{G12D/+}$ mice. (**e**) Occurrence of extrapancreatic tumors in KF mice. Scale bars, 50 μm.

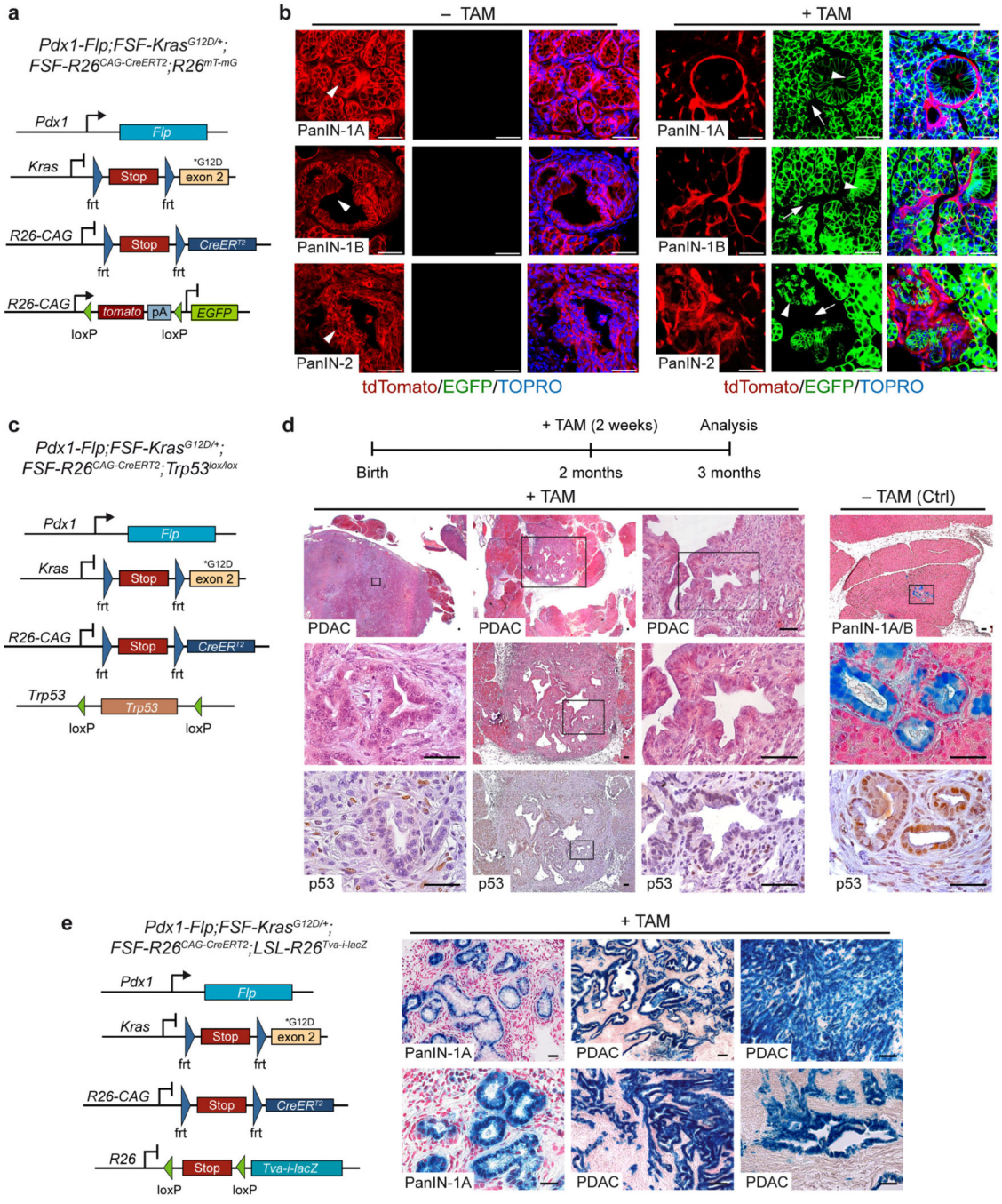


**Figure 2.**

Secondary genetic manipulation of established Kras$^{G12D}$-induced PanIN lesions and PDAC cells in the *Pdx1-Flp* lineage. (**a**) Genetic strategy to induce EGFP expression in the Flp lineage by tamoxifen-mediated activation of CreER$^{T2}$. (**b**) Representative confocal microscopic images of tdTomato (red, non–Cre-recombined cells) and Cre-induced EGFP (green) expression in the pancreas and indicated PanIN lesions of tamoxifen- (+TAM) and vehicle-treated (–TAM) male and female mice. Arrowheads indicate highest-grade PanIN lesions; arrows indicate stromal cells. Nuclei were counterstained with TOPRO-3 (blue). (**c**)

Genetic strategy to recapitulate human multistep carcinogenesis by time-specific *p53* inactivation. (**d**) Top, schematic of tamoxifen treatment protocol. Bottom, representative alcian blue (blue) and H&E-stained pancreatic tissue sections of randomized tamoxifen-treated *Pdx1-Flp*;*FSF-Kras*$^{G12D/+}$;*FSF-R26*$^{CAG\text{-}CreERT2/+}$;*Trp53*$^{lox/lox}$ mice (+TAM) and untreated age- and sex-matched littermate controls (–TAM). *n* = 3 mice per group. Bottom, immunohistochemical p53 staining demonstrates loss of p53 expression in TAM-treated tumors but not in untreated controls. (**e**) Genetic strategy to induce *lacZ* expression by tamoxifen-mediated CreER$^{T2}$ activation (left). Right, representative β-galactosidase staining (n = 3 representative slides from three mice) shows expression of *lacZ* in PanIN lesions and PDAC, but not in desmoplastic stroma of tamoxifen-treated male and female *Pdx1-Flp*;*FSFKras*$^{G12D/+}$;*FSF-R26*$^{CAG\text{-}CreERT2}$;*LSL-R26*$^{Tva\text{-}i\text{-}lacZ}$ mice. Scale bars, 50 μm.

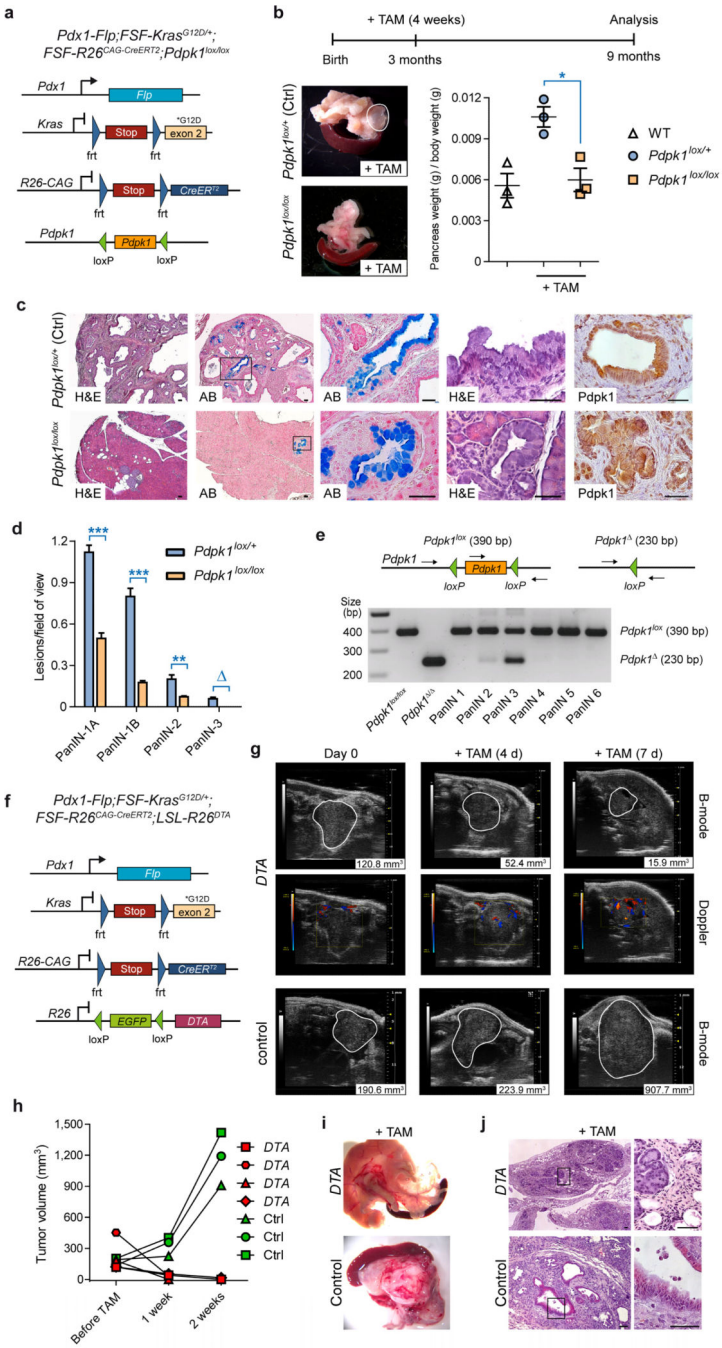


**Figure 3.**

Validation of therapeutic targets *in vivo* by Cre-induced time-specific *Pdpk1* inactivation or DTA-mediated tumor cell depletion. (**a**) Genetic strategy to delete *Pdpk1* in established PanIN lesions by time-specific tamoxifen-mediated CreER$^{T2}$ activation. (**b**) Top, schematic of tamoxifen (TAM) treatment protocol. Bottom, representative macroscopic view (left) and weight (right) of pancreata from TAM-treated homozygous conditional *Pdpk1*-knockout mice (*Pdpk1*$^{lox/lox}$) and age- and sex-matched TAM-treated heterozygous controls (*Pdpk1*$^{lox/+}$). Visible tumors are outlined in white. WT, wild type. Data represent mean ±

s.e.m; $n = 3$ female mice per genotype; $^{*}P = 0.0148$, Student's $t$ test. (**c**) Representative pancreatic sections of TAM-treated *Pdpk1*$^{lox/+}$ control (top) and *Pdpk1*$^{lox/lox}$ (bottom) mice stained with standard H&E or alcian blue (AB) to visualize mucinous PanIN lesions stained in blue and immunohistochemical Pdpk1 staining. (**d**) Absolute quantification of different grades of PanIN lesions (grade −1A, flat epithelial lesion; grade −1B, papillary lesion; grade −2, lesion with nuclear abnormalities; grade −3, carcinoma in situ) in 9-month-old sex-matched TAM-treated mice with genotypes as indicated (mean and s.e.m.; $n = 3$ female mice per genotype; 3 representative slides per mouse; $^{***}P < 0.001$, $^{**}P < 0.01$, Student's $t$ test; $^{\Delta}P = 0.05$, Fisher's exact test). (**e**) Top, genotyping strategy to detect *Pdpk1* alleles. Bottom, PCR analysis of nonrecombined *Pdpk1*$^{lox/lox}$ DNA from a mouse without Cre expression, recombined pancreatic tissue from a *Ptf1a*$^{Cre/+}$;*LSL-Kras*$^{G12D/+}$;*Pdpk1*$^{lox/lox}$ (*Pdpk1*$^{\Delta/\Delta}$;[17]) mouse (positive control for recombined allele) and microdissected PanIN lesions from TAM-treated *Pdpk1*$^{lox/lox}$ mice. (**f**) Genetic strategy to induce DTA expression in established PDAC by tamoxifen-mediated CreER$^{T2}$ activation. (**g**) Tumor growth was monitored by high-resolution ultrasound in sex-matched DTA and control mice with mean tumor diameters >5 mm before (day 0) and 4 and 7 d after treatment with tamoxifen (+TAM). Macroscopic tumor perfusion was evaluated by Doppler ultrasound. Visible lesions are outlined in white; numbers (bottom right corner) indicate tumor burden as determined by automated three-dimensional B-mode imaging. (**h**) Quantification of tumor volume in TAM-treated DTA ($n = 4$) and control (Ctrl, $n = 3$) mice. (**i**) Representative macroscopic view of pancreas from TAM-treated DTA (top) and control (bottom) mouse. (**j**) Representative H&E stains of TAM-treated DTA (top) and control (bottom) mouse. Scale bars, 50 μm.

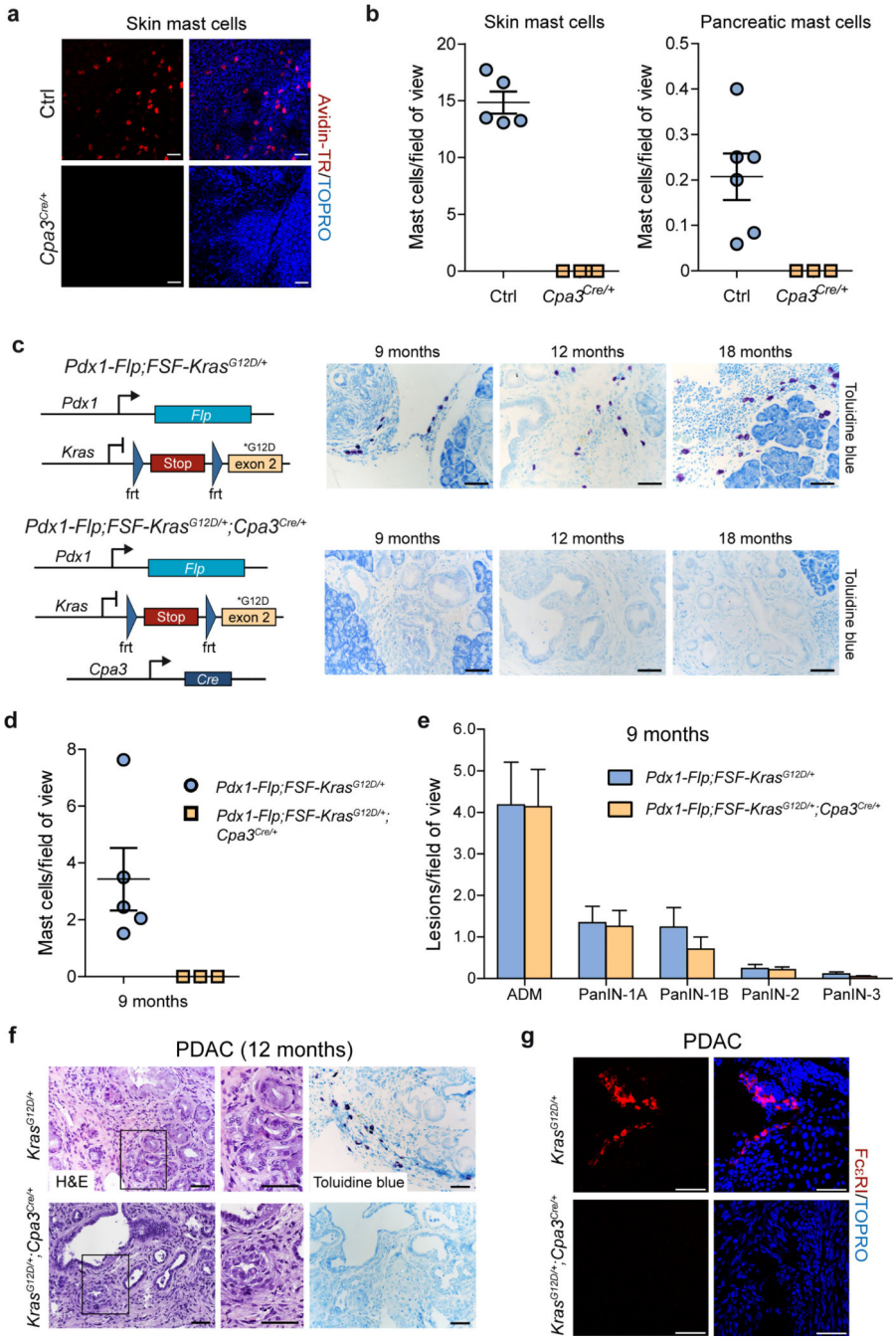


**Figure 4.**

Mast cells are dispensable for PDAC development. (**a**) Representative confocal microscopic images of skin whole-mounts of male *Cpa3*$^{Cre/+}$ and littermate control (Ctrl) mice on a *C57BL/6* genetic background. Mast cells were stained with avidin-TexasRed (red) and nuclei were counterstained with TOPRO-3 (blue). (**b**) Quantification of skin (left) and pancreatic (right) mast cells in male and female *Cpa3*$^{Cre/+}$ and control mice (mean, ± s.e.m.; 10–15 fields of view per animal; each dot in the graph represents one mouse). (**c**) Genetic strategy to eradicate mast cells in the KF model by Cre recombinase expression using

*Cpa3*$^{Cre/+}$ mice (left). Representative images of toluidine blue–stained metachromatic mast cells (purple) in PanIN-bearing pancreata of male and female KF (top) and mast cell-depleted *Pdx1-Flp*;*FSF-Kras*$^{G12D/+}$;*Cpa3*$^{Cre/+}$ (bottom) mice ($n$ = 3 animals per genotype). (**d**) Quantification of tumor-infiltrating mast cells in 9-month-old PanIN-bearing male and female mice with genotypes as indicated (mean ± s.e.m.; 15 fields of view per animal). (**e**) Absolute quantification of ADM and different grades of PanIN lesions in 9-month-old male and female *Pdx1-Flp*;*FSF-Kras*$^{G12D/+}$;*Cpa3*$^{Cre/+}$ ($n$ = 3) and *Pdx1-Flp*;*FSF-Kras*$^{G12D/+}$ ($n$ = 4) mice (mean and s.e.m.; three representative slides per mouse). (**f**) Representative H&E and toluidine blue staining of tissue sections from 12-month-old male *Pdx1-Flp*;*FSF-Kras*$^{G12D/+}$ (top) and *Pdx1-Flp*;*FSF-Kras*$^{G12D/+}$;*Cpa3*$^{Cre/+}$ mouse with established PDAC (three representative slides per mouse). (**g**) Representative immunofluorescence staining of FcεRI (red) in mast cells in PDAC-bearing male *Pdx1-Flp*;*FSF-Kras*$^{G12D/+}$ (top) and *Pdx1-Flp*;*FSF-Kras*$^{G12D/+}$;*Cpa3*$^{Cre/+}$ (bottom) mouse (three representative slides per mouse). Nuclei are counterstained with TOPRO-3 (blue). Scale bars, 50 μm.

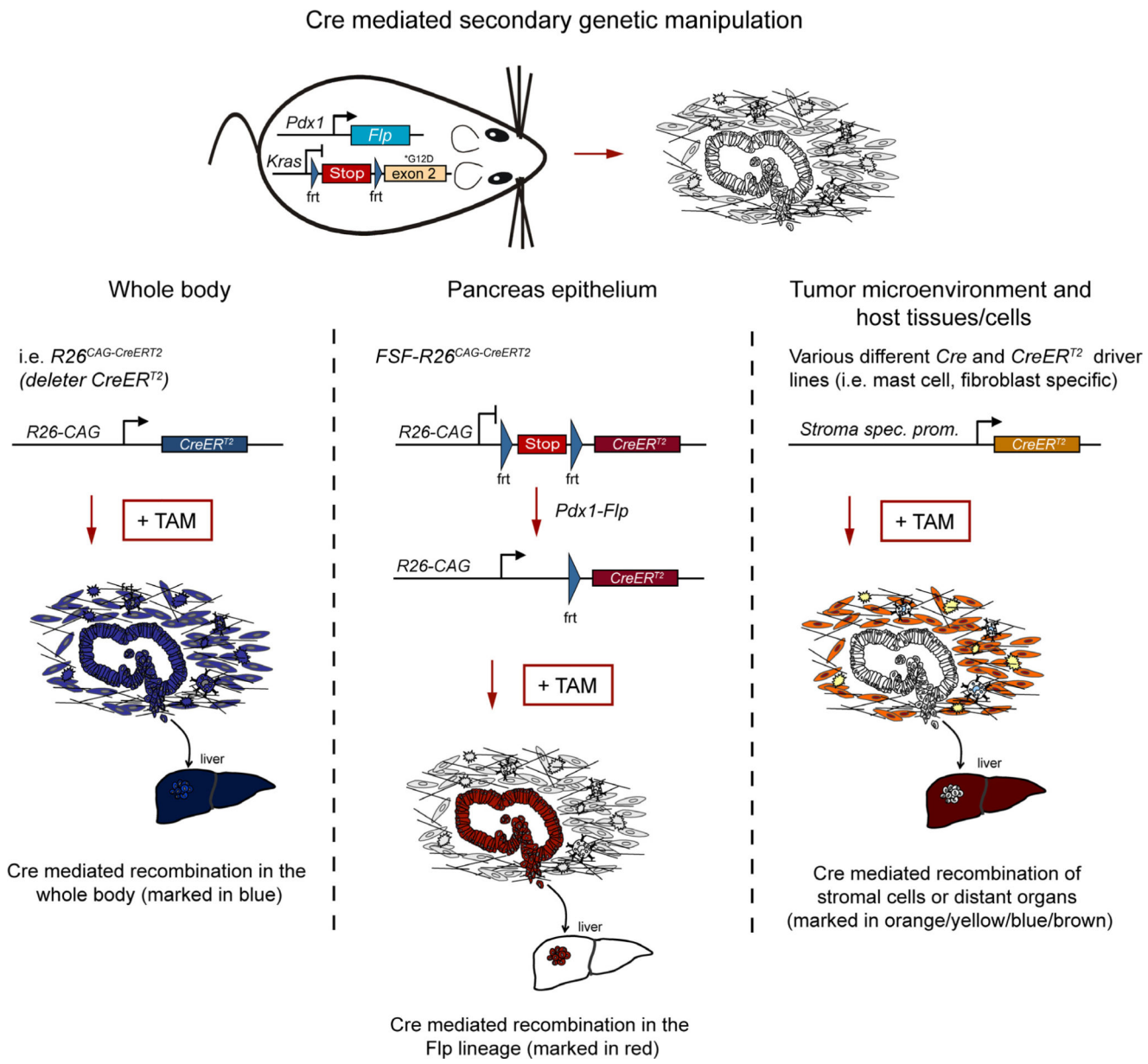


**Figure 5.**

Applications of DRS. Stroma-rich PDAC tumors can be induced by *Pdx1-Flp*– mediated activation of an *FRT*-stop-*FRT* (FSF) silenced oncogenic $Kras^{G12D}$ allele in the pancreas. Middle, secondary genetic manipulation of tumor cells in the Flp lineage can be achieved by a FSF-silenced latent $CreER^{T2}$ allele ($FSF\text{-}R26^{CAG\text{-}CreERT2}$). $CreER^{T2}$ can be activated by tamoxifen treatment at any time point during tumor formation and progression to recombine floxed sequences. In this way it is possible to model and analyze multistep carcinogenesis, manipulate tumor subpopulations, validate therapeutic targets in established tumors and analyze resistance mechanisms by genetic approaches. The use of various Flp driver lines or a Flp-expressing virus allows expression of oncogenic $Kras^{G12D}$ or any other Flp-*FRT*-regulated oncogene or tumor suppressor in various different tissue and cell types. Left, use of a $CreER^{T2}$ deleter allele, which is expressed from the *Rosa26* locus under the control of

the *CAG* promoter in all cells of the body, allows whole-organism, time-specific deletion of a target or pathway, making it possible to mimic drug treatment and thus evaluate its value as a drug target for therapy of established PDAC. Right, Cre driver lines and expression models can be used to target subpopulations of the tumor microenvironment, such as fibroblasts (orange), stellate cells (yellow), endothelial cells, pericytes, adipocytes and mast cells (blue), as well as other immune cells. In addition, metastasis target organs and the metastatic niche and other host factors, tissues and cells can be genetically manipulated.